Journal of Materials Chemistry C

Accepted Manuscript

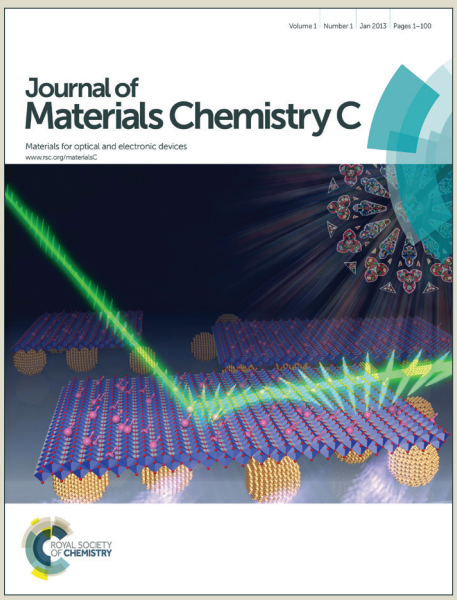

ROYAL SOCIETY OF CHEMISTRY

www.rsc.org/materialsC

Journal Name

RSCPublishing

ARTICLE

Ladder-type Conjugated Oligomers Prepared by Scholl Oxidative Cyclodehydrogenation Reaction: Synthesis, Characterization and Application in Field Effect Transistor

Wei Huang, Hejian Zhang, Ji Ma, Moyun Chen, Haoyun Zhu and Weizhi Wang*

Two novel well defined ladder-type conjugated oligomers have been successfully designed and synthesized through a solution processing method in an excellent yield. And the field effect transistors (FETs) fabricated by these ladder-type oligomers with nice planar structure exhibit excellent charge carrier mobility up to 0.10 $cm^2V^{-1}s^{-1}$ and 0.33 $cm^2V^{-1}s^{-1}$, furthermore the devices can work well with a low gate voltage. The ladder-type oligomers are both converted from two precursor co-oligomers poly(2,7-(1,2,-diphenylethene)-9,9-dioctylfluorene) (**PDPF**) via an anhydrous $FeCl_3$ oxidative cyclodehydrogenation. The pronounced red shift shown in the preliminary photoluminescence spectra and the changes of band gaps measured by electrochemical analysis, both testify that the better electronic transmission capacity in FET performance is due to the expanded molecular chains planarization after the chemical cyclodehydrogenation. Interestingly, the precursor oligomers owning a linear-type chain and a zigzag-type chain respectively (**L-PDPF** and **Z-PDPF**) show lots of characteristic differences in thermal, optical and electrochemical properties. The differences caused by the diverse types of main chains demonstrate that the macromolecular configurations have tremendous impact on the functioning of the oligomers.

Introduction

Graphene as a promising two dimensional material has attracted great interest for a wide range of electronic applications and the related research is developing rapidly in recent years.[1-7] It could be attained by a great deal of physical methods such as the mechanical exfoliation of graphite[8], the unzipping of carbon nanotubes[9], lithography[10] and the reduction of graphite oxide[11]. Inspired by these developments, many research groups have devoted plenty of effort to the design and synthesis of diverse graphene-like materials in the fields of oligomers and macromolecules.[12-17] During these researches, the conjugated oligomer is a category of significant material. The applications of conjugated oligomers in photovoltaic cells, electroluminescent diodes, thin film transistors and chemical sensors have been paid more and more attentions.[18-23] Compared to the small molecules, the conjugated oligomers especially with ribbon- or ladder-type framework not only form graphene-like structures, also possess some unique characteristics such as largely defect-free accurate structure and excellent film forming property.[24,25] In addition, unlike the zero-band gap graphene, the ladder-type conjugated oligomers (LCOs) with different band gaps show their outstanding semiconducting nature fitting to be applied in manifold electronic devices as the active materials.[26-28]

Up to now there exist two principal chemical methods to synthesize the ladder-type materials: one is the polymerization of some multifunctional monomers, generating a ladder type just in one single reaction; and the other is the cyclization of suitably functionalized open-chain precursor in a polymer-homologous process.[29-32] Compared with the physical methods, chemical synthesis could precisely control the structure with the desired shape and dimension of the achieved products. Because of its more atom-economical and straightforward, the late-stage cyclization by the direct transformation of C–H bonds have been studied by many chemists.[33-35] K. Müllen's group[36,37] and W. R. Dichtel's group[38] have both employed an efficient way to prepare well defined polycyclic aromatic hydrocarbons by the Scholl oxidative cyclodehydrogenation reaction, in which a kind of precursor for potential graphene-like molecule is oxidized by iron(III) chloride ($FeCl_3$)/nitromethane system. Inspired by the above examples and the properties of LCOs, we propose to develop a method for synthesizing a sort of novel LCOs to overcome the drawbacks of the small molecules. Moreover, the LCOs will be applied to manufacture high-performance semiconductor devices like FETs.[39,40]

In this work, 9,9-dioctylfluorene and two isomers of 1,2-diphenylethene are chosen as the monomeric units. The reason for combining fluorene is that the fluorene-based polymers have exhibited favourable chemical and thermal stability, exceptionally high photoluminescence and electroluminescence fluorescent quantum efficiency in thin solid films.[41-45] Moreover, the long alkyls

State Key Laboratory of Molecular Engineering of Polymers, Department of Macromolecular Science, Fudan University, Shanghai 200433, P. R. China. E-mail: weizhiwang@fudan.edu.cn; Tel: +86 021-65643836

†Electronic supplementary information (ESI) available: experimental section including materials, measurements and characterizations; mass spectra, NMR data for new compounds and oligomers, cyclic voltammetry figures, GPC data for the oligomers and CCDC reference numbers 1043775-1043776. For ESI or other electronic format see DOI: 10.1039/x0xx00000x

in the 9th position of the fluorene unit can make the target oligomers render good solubility in common organic solvents. Prior to the polymerization, the 1,2-diphenylethene monomers of *cis-trans* isomerism were successfully synthesized, thus the isomers were used to obtain two alternating co-oligomers only differing on their configurations: one is (*E*)-poly(2,7-(1,2,-diphenylethene)-9,9-dioctylfluorene) (**L-PDPF**) which owns a linear-type chain and the other (*Z*)-poly(2,7-(1,2,-diphenylethene)-9,9-dioctylfluorene) (**Z-PDPF**) has a zigzag-type chain. Interestingly, the disparate emission fluorescent colours of these two oligomers under the same UV irradiation inspire us to consider the influence of the different configurations on their performance as well. Therefore, we further investigate how the diverse configurations affect the properties of these oligomers. Most importantly, **L-PDPF** and **Z-PDPF** can be converted into the oligomers with a ladder type (**L-PDPF-O** and **Z-PDPF-O**) after the $FeCl_3$ oxidation. Accordingly, the corresponding model molecules of the precursor oligomers, (*E*)-1,2-diphenylethene-1,2-bis(9,9-dioctyl-9H-fluoren-2-yl) (**L-DPBF**), (*Z*)-1,2-diphenylethene-1,2-bis(9,9-dioctyl-9H-fluoren-2-yl) (**Z-DPBF**) and their oxidations **L-DPBF-O** and **Z-DPBF-O** are synthesized to elucidate the cyclodehydrogenation. The efficient planarization of the precursor oligomers into the LCOs is corroborated by ^{1}H NMR and FT-IR spectra. Subsequently, these LCOs have been fabricated in FETs as the semiconductor layer to measure the performance. Additionally, the relevant properties to prove whether the intramolecular cyclization enhance the electronic transmission capacity by extending the molecular plane are all discussed as well in this work.

Results and discussions

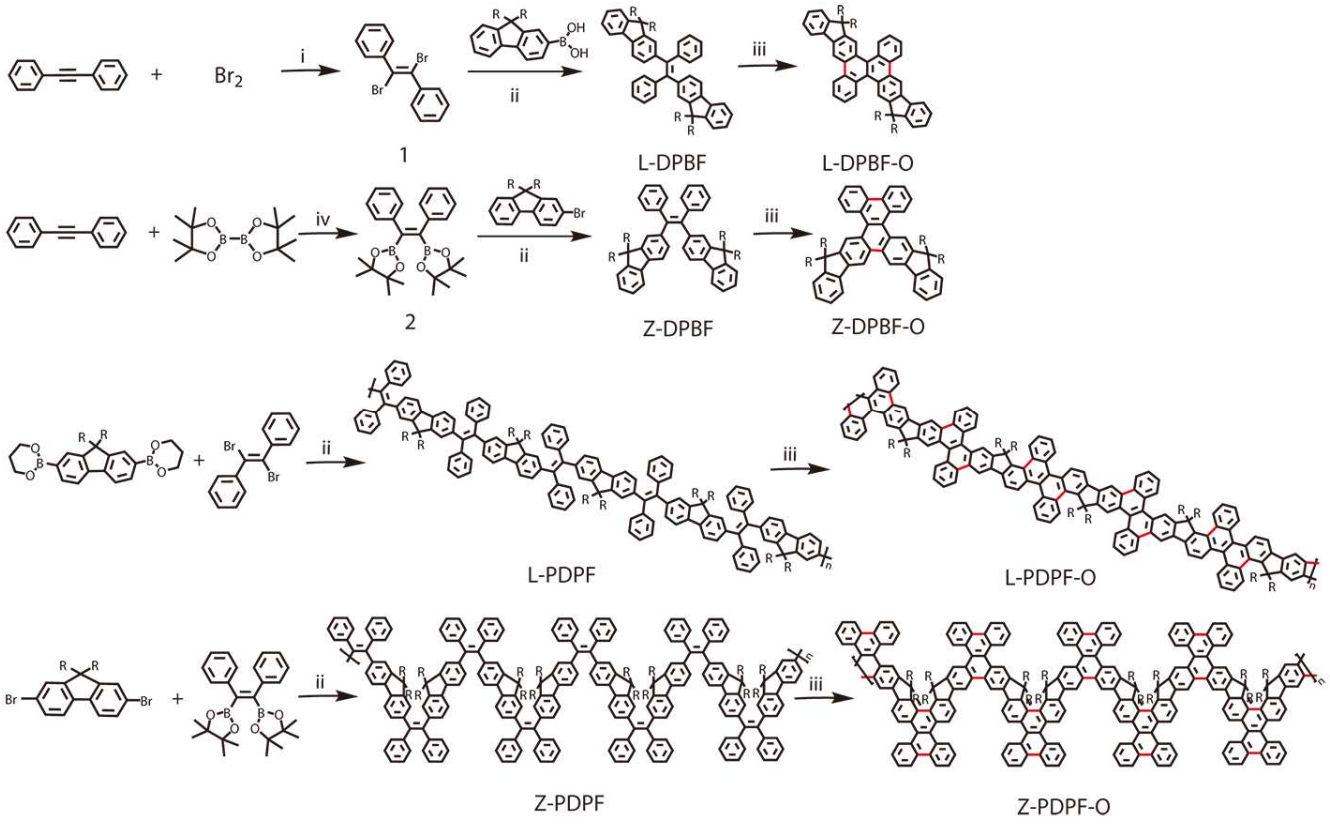

Scheme 1 Synthetic approaches of monomers, model molecules and oligomers. i. CCl_4, -12 °C / 1h; ii. $Pd(PPh_3)_4$ / K_2CO_3, toluene/H_2O, 95 °C / 5 days; iii. $FeCl_3$, CH_2Cl_2/CH_3NO_2, room temperature / overnight; iv. $Pt(PPh_3)_4$, DMF, 90 °C / 24 h. R: C_8H_{17}.

The overall synthetic procedures toward model molecules, monomers and oligomers are clearly outlined in Scheme 1. It is easy to see that the linkage ways of 1,2-diphenylethene in the obtained **L-PDPF** and **Z-PDPF** are actually *cis-trans* isomerism, so these two precursor oligomers own different main chain configurations. To acquire these two configurations, the monomer **1** and **2** are directly synthesized according to the methods described in the literatures.[46,47] What is more, the pure single crystals of these monomers are both fortunately recrystallized from their CH_2Cl_2/n-hexane solution. The accurate structures of **1** and **2** are identified by X-ray crystallographic analysis in Fig. 1 plus the data in supporting information (Table S1). Another fluorene derivative monomer, 2,7-dibromo-9,9-dioctylfluorene, has been prepared in advance as reported.[48] Normally, the long alkyl chains in the 9th position can enhance the solubility of the oligomer in organic solvents like THF and toluene, which allows a solution-processing so is beneficial to the degree of polymerization.

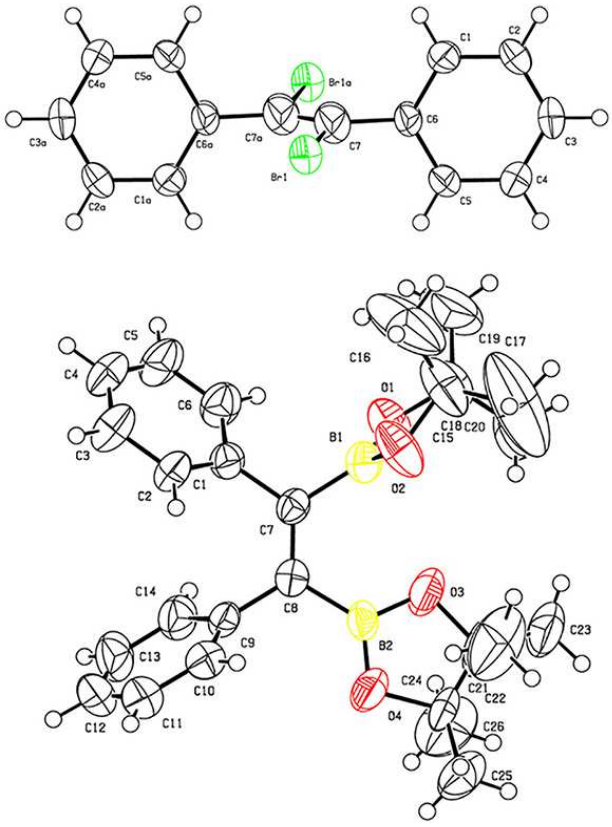

Fig. 1 The ORTEP drawing of **1** and **2**.

Then the elemental approach employed for the synthesis of the precursor is a Suzuki cross-coupling reaction[49] as the description in Scheme 1. Evidently, the difference of these two oligomers is that **L-PDPF** presents a linear-type main chain and **Z-PDPF** has a zigzag-type chain as pictured in the schematic. The much more flexible zigzag-type chain enables the building blocks in its twisted chain to rotate more easily. As displayed in Table 1, the M_w values of **L-PDPF** and **Z-PDPF** are determined by gel permeation chromatography (GPC, Fig. S1 and Fig. S2) with THF as the eluent and polystyrene as the standard to be 9900 and 6800. Their polydispersity indices (PDIs) calculated by means of M_w/M_n are 1.32 and 1.36 respectively. THF and toluene are both proven as the solvent in the polymerization. The reaction temperature is 60 °C when the solvent is THF, which guides to the products with a lower degree of polymerization. The molecular mass is increasing obviously when toluene is selected to replace THF and the reaction temperature is brought upwards to 95 °C. It's likely due to the low temperature influencing negatively the activities of the monomers, which results in a deviation of their actual concentration ratio in solution, thereby the monomers could not react at an envisioned proportion in this alternating copolymerization.

After that we expect to attain the LCOs with bigger conjugated planarization via one-step chemical cyclization. An efficient reaction route named Scholl reaction on the basis of the reference[50] is adopted. Herein, the anhydrous $FeCl_3$ is utilized as an oxidant for these transformations, which has been used for the synthesis of the polycyclic aromatic hydrocarbon because of its restraining from severe disadvantages such as dealkylation, chlorination or migration of the alkyl substituents.[51] In the end, methanol is poured into the mixture to consume the extra anhydrous $FeCl_3$ and the oxidized products are purified through column chromatography.

Table 1. Molecular weights of **L-PDPF** and **Z-PDPF**

Oligomer	Yield	Colour	Mw	PDIs
L-PDPF	44.7%	Yellow Green	9900	1.32
Z-PDPF	52%	Yellow	6800	1.36

All these prepared monomers and final products are carefully purified and further characterized by nuclear magnetic resonance spectra (NMR) and the successful intramolecular cyclization can be presented by these ^{1}H NMR spectra. As an instance, the ^{1}H NMR spectra of **Z-PDPF** and **Z-PDPF-O** are revealed in Fig. 2a. It is pronounced that the peaks within 7~8 range representing the hydrogen on the phenyl rings weaken drastically after the oxidative cyclodehydrogenation, which might indicate the formation of C-C bonds between the phenyl rings to produce more six-member rings in the backbones to take on a ladder-type structure. The detailed ^{1}H NMR spectra of the model compounds **(Z-DPBF** and **Z-DPBF-O)** in the supporting information (Fig. S20 and Fig. S21) demonstrate clearly the cyclization between the substituted phenyl rings. Simultaneously, the corresponding ^{1}H NMR spectra of the products in the **L-PDPF** system exhibit the same trend. The complete ^{1}H NMR and ^{13}C NMR spectra of all these synthesized products implied in the supporting information (Fig. S3 – S22) could also be further evidence to illustrate the success of these syntheses. Moreover, the decline of the aromatic protons signals after the cyclization is reported in the references.[15,16,37] However, the reason is short of a reliable and reasonable explanation till now. A variable-temperature experiment (25 °C to 50 °C) of **Z-PDPF-O** in 1,1,2,2-tetrachloroethane-d2 solution has been carried out. (Fig. S23) The unchanged spectra at different temperatures indicate that the chemical shifts of the aromatic resonances are independent of temperature, and it is not attributed to the aggregation.

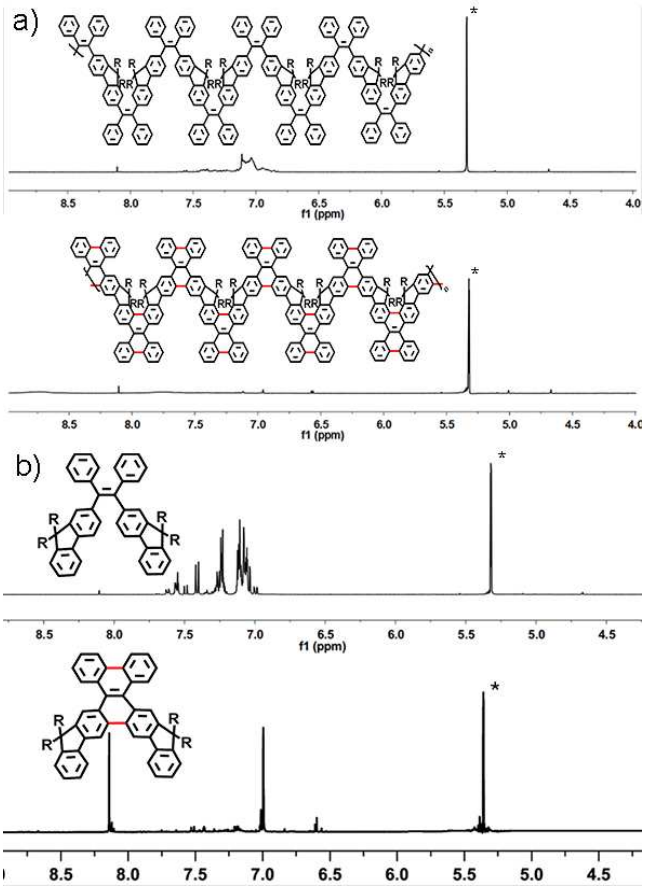

Fig. 2 (a) ^{1}H NMR spectra of **Z-PDPF** and **Z-PDPF-O**; (b) ^{1}H NMR spectra of **Z-DPBF** and **Z-DPBF-O**. R: C_8H_{17}.

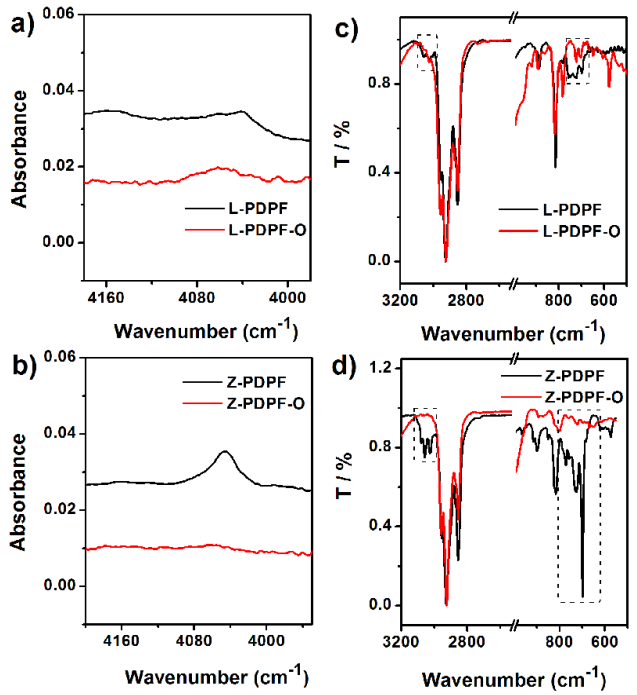

Fig. 3 (a) Part of FT-IR spectra within the near infrared region (4000~4200 cm^{-1}) of **L-PDPF** and **L-PDPF-O**; (b) Part of FT-IR spectra within the near infrared region (4000~4200 cm^{-1}) of **Z-PDPF** and **Z-PDPF-O**. (c) Part of the FT-IR spectra within the middle infrared regions (550~1120 cm^{-1}, 2550~3250 cm^{-1}) of **L-PDPF** and **L-PDPF-O**; (d) Part of the FT-IR spectra within the middle infrared regions (550~1120 cm^{-1}, 2550~3250 cm^{-1}) of **Z-PDPF** and **Z-PDPF-O**. *T* means transmissivity.

Moreover, the mass spectrometric data of small molecules like **1**, **2** and the model molecules are used to demonstrate the successful synthesis in supporting information (Fig. S24 – S29). The divergences in the mass spectral data between the model molecules before and after chemical oxidation also testify the successful synthesis of the expected oxidized products. Four hydrogens are precisely removed after the oxidation. Also, the cyclization processing can be further confirmed by the detection of Fourier transform infrared (FT-IR) as displayed in Fig. 3. From Fig. 3a and Fig. 3b, the band at about 4050 cm^{-1} can be taken as a palpable marker of the existence of the free rotating phenyl rings in the molecules[36], therefore, is distinctly observed in the spectra of **L-PDPF** and **Z-PDPF**. The disappearance of this peak in the spectra of the obtained LCOs indicates the absence of the hydrogens on the substituted phenyl rings. Altogether these changes after the cyclodehydrogenation demonstrate the restrictions to the gestures of the substituted phenyl rings. Additionally, in Fig. 3c and Fig. 3d, the pronounced disappearance of the characteristic peaks of these oligomers can be observed before and after the oxidation. Some reveal the disappearance of these out of plane C–H deformation bands at 698, 728 and 775 cm^{-1}, which are typical for mono- and disubstituted phenyl rings. And the noticeable triad peaks of the aromatic C–H stretching vibrations at 3023, 3056 and 3079 cm^{-1} are attenuated, which verifies the efficient conversion from **PDPF** into **PDPF-O**.

UV-vis absorptions and photoluminescence (PL) data of the oligomers in THF are listed in Table 2. The **L-PDPF-O** displays an absorption wavelength (λ_{abs}) at 405 nm, resulting in a 3 nm red shift compared with that of **L-PDPF**. The related absorption spectra of the obtained oligomers are displayed in the supporting information. (Fig. S30) And their PL spectra have a same red-shifted behaviour with the emission peak moving from 418 nm to 447 nm. For **Z-PDPF** and its oxidized product **Z-PDPF-O**, the corresponding spectral shift shows a similar trend: the absorption maximum of **Z-PDPF** is at 420 nm, together with 451 nm of **Z-PDPF-O**. Furthermore, their emission wavelengths exhibit a similar red shift from 498 nm to 551 nm. All of these bathochromic-shifted tendencies indicate that the broader planarization of the molecular chain and the conjugated degree after the oxidation is increasing because of the cyclization between the substituted phenyl rings. PL efficiencies (Φ_F) of oligomers are measured in dilute THF solution using quinine sulfate (Φ_F = 0.54 in 0.1 M sulfuric acid solution) or fluorescein (Φ_F = 92% in 0.1M NaOH solution) as a reference. The Φ_F of **L-PDPF** is high of 81.7% compared to that of **Z-PDPF** merely having 3.1%.

Table 2 The UV-vis absorptions and PL data of the oligomers in THF solution.

Oligomer	λ_{abs} [a] (nm)	λ_{em} [b](nm)	ΔS [c] (nm)	Φ_F [d] (%)	τ [e] (ns)
L-PDPF	402	418	16	81.7	0.501
L-PDPF-O	405	447	42	62.9	0.507
Z-PDPF	420	498	78	3.07	1.114
Z-PDPF-O	451	551	100	39.5	1.988

[a] Absorption maximum. [b] Emission maximum. [c] Stokes shift calculated from the absorption and emission spectra. [d] Quantum yield estimated with quinine sulfate (Φ_F = 54% in 0.1 M H_2SO_4) or fluorescein (Φ_F = 92% in 0.1 M NaOH) as standards. [e] Fluorescent lifetime.

It could be observed intuitively by our naked eyes from Fig. 4a that **L-PDPF** emits luminous blue light, meanwhile **Z-PDPF** emits faint yellow light under the same 365 nm UV irradiation. We consider the tremendous intensity difference is induced by the molecular configurations. The zigzag chains of **Z-PDPF** are more flexible than the linear chains of **L-PDPF**, so the zigzag chains can deactivate excited species through nonradiative rotations to consume the excited energy. Later after the cyclization, **L-PDPF-O** emits purple fluorescent light and **Z-PDPF-O** emits redder light with stronger intensity as expressed in Fig. 4b, which is consistent with the red-shifted behaviour as noted earlier. The stronger intensity of **Z-PDPF-O** owes to the broader planarization for promoting the rigidity of the zigzag chains to hinder the rotations of the building units so that more excited energy is consumed by emitting light. The lifetime (τ) of **L-PDPF-O** is 0.507 ns as much as 0.501 ns of **L-PDPF**. However, τ of **Z-PDPF-O** is 1.988 ns compared to 1.114 ns of **Z-PDPF** which shows more changes after the oxidation. This is likewise due to the stronger rigidity of the chains after the intramolecular cyclization as well. In addition, the inserted photograph of Fig. 4c shows the emitting light of all the four oligomers in the solid state. The **L-PDPF** emits a green light and **Z-PDPF** emits a strong yellow light. Through the comparison between Fig. 4a and the inserted photograph in Fig. 4c**, Z-PDPF** has a remarkable aggregation-induced emission (AIE) phenomenon: some non-luminance dyes can be induced to emit light effectively by the aggregated formation.[52,53] The changed fluorescent lifetime and the AIE phenomena are both caused by steric interactions in the materials. Parts of the chains of **Z-PDPF** are able to pack closer through π-π stacking process owing to their twisted zigzag shape, which weakens the transferring electronic quenching. At the same time, the rotations of segments in their chains are mainly restricted due to the physical constraint. This restriction of intramolecular rotations blocks the nonradiative pathways and opens up a radiative channel. As a result, **Z-PDPF** becomes emissive in the solid state. From this photograph, **L-PDPF-O** and **Z-PDPF-O** in solid state both show red-shift to emit redder light as we anticipated in advance.

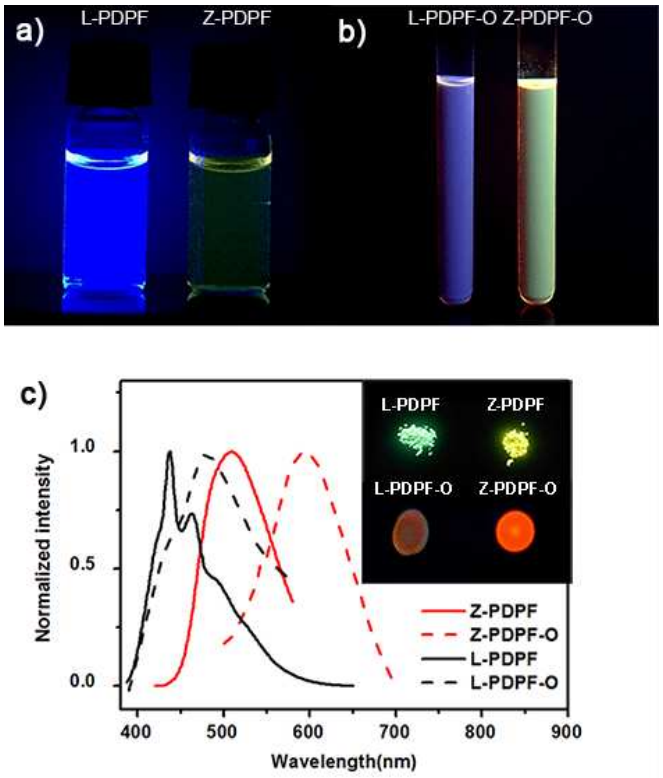

Fig. 4 (a) The pictures of **L-PDPF** and **Z-PDPF** in THF solution under 365 nm UV irradiation; (b) The photographs of **L-PDPF-O** and **Z-PDPF-O** in THF solution under 365 nm UV irradiation. (c) PL spectra of **Z-PDPF**, **Z-PDPF-O**, **L-PDPF** and **L-PDPF-O** in the solid state. The inserted image in panel c: the photograph of **L-PDPF**, **L-PDPF-O**, **Z-PDPF** and **Z-PDPF-O** in solid state under 365 nm UV irradiation.

Likewise in the inserted photograph we can observe directly that **Z-PDPF-O** on the right possess redder light with stronger intensity. The further proof to illustrate this phenomenon is the PL emission spectra of oligomers in the solid state from Fig. 4c. **L-PDPF-O** shows a red shift from 438 nm to 480 nm while **Z-PDPF-O** has a longer wavelength emission light at 595 nm compared to 510 nm. The emission wavelength of **Z-PDPF-O** is indeed closer to the visible red light range. It's supposed that the intramolecular cyclization broaden the conjugated plane in

the backbones of the LCOs to boost electrons transmission in the delocalization**.** Although there are still some rotations between different segments, the chemical oxidation expands the cofacial surface at different rotation degree on the main chain to result in a bigger conjugated planarity in the whole molecules. According to the studies carried out by F. Cacialli[48] and A. C. Grimsdale[49], the ratio of *cis*-linkage in the main chains can influence the emission wavelength and the oligomer consist of more *cis*-1,2-diphenylethene has been found to exhibit a more pronounced red-shift of the emission wavelength. The PL measurements in our work are consistent with this phenomenon as well, which show that **Z-PDPF** and **Z-PDPF-O** with *cis*-1,2-diphenylethlene in the repeat units both emit longer wavelength light in solid state than **L-PDPF** and **L-PDPF-O**.

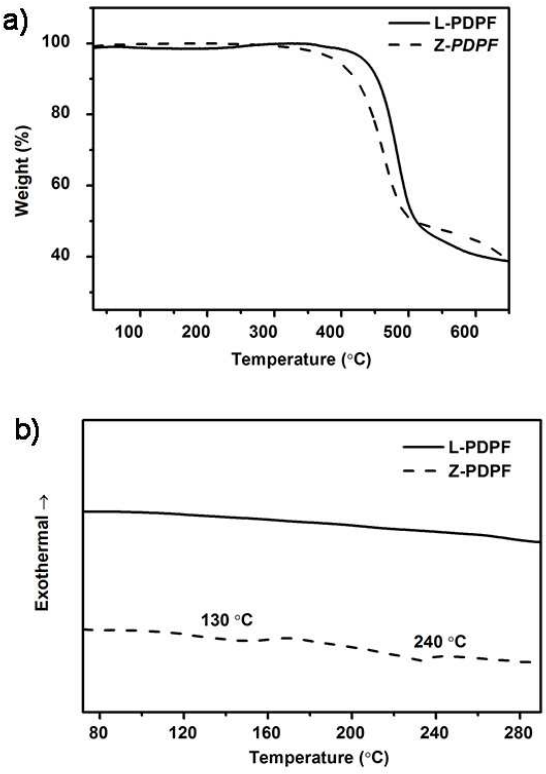

Fig. 5 (a) The TGA data of **L-PDPF** and **Z-PDPF**; (b) The DSC data of **L-PDPF** and **Z-PDPF**.

The thermal properties of the synthesized oligomers **L-PDPF** and **Z-PDPF** measured by thermal gravimetric analysis (TGA) in N_2 both show marvellous thermal stability. The onset decomposition temperature of **L-PDPF** is 415 °C and the other one is 419 °C as illustrated in Fig. 5a. Nevertheless, the differential scanning calorimetry (DSC) measurements (Fig. 5b) exhibit clear divergence that **Z-PDPF** has a glass transformation at around 130 °C and 240 °C however **L-PDPF** does not have a glass transformation during the measured temperature range. This difference in the glass transformation indicates that the main chain of **Z-PDPF** in the solid state is more flexible than **L-PDPF**, which leads to significant relationships with the linear and nonlinear configurations because of the *trans*- and *cis*- linkage of 1,2-diphenylethene. The more twisted zigzag shape configuration of **Z-PDPF** chain increases the intermolecular interactions like π-π packing to make up more crystalline regions, which makes it manifest some glass transformations. However, the rigid linear chains of **L-PDPF** are less flexible to form the amorphous instead of the ordered crystallization, so there is no glass-transition temperature.

To explore the electrochemical redox behaviour of the oligomers, it's well known that the lowest unoccupied molecular orbital (LUMO), the highest occupied molecular orbital (HOMO) and energy band gaps (ΔE_g) are three crucial parameters for electroluminescent materials. In order to better understand the relationship between the electronic structure and the optical properties, meanwhile to explain the pronounced fluorescence red-shift, cyclic voltammetry analyses of the synthesized compounds coated on a glassy carbon electrode were carried out in an electrolyte of 0.1 M tetrabutylammonium hexafluorophosphate ($TBAPF_6$) in acetonitrile using ferrocene as the internal standard at a scan rate of 100 mV/s at room temperature under the protection of argon. An $Ag/AgNO_3$ electrode was used as the reference electrode and a Pt wire was applied as the counter electrode. According to the empirical relationships, the HOMO value can be derived by the equation: HOMO = -e($E_{onset\text{-}ox}$-0.0468 V)-4.8 eV, where $E_{onset\text{-}ox}$ is the onset oxidation potential determined from cyclic voltammetry in acetonitrile for oxidation potentials and the value 0.0468 V is for FOC vs Ag/Ag^+. LUMO = ΔE_g + HOMO. The corresponding data of the oligomers are summarized in Table 3, and the cyclic voltammograms can be found in the supporting information (Fig. S31).

Table 3 Electrochemical properties of **L-PDPF**, **L-PDPF-O**, **Z-PDPF** and **Z-PDPF-O**

Oligomer	E_g(eV)	HOMO(eV)	$E_{onset\text{-}ox}$ (V)	LUMO(eV)
L-PDPF	3.00	-5.73	0.98	-2.73
L-PDPF-O	2.74	-5.55	0.80	-2.81
Z-PDPF	2.81	-5.58	0.82	-2.77
Z-PDPF-O	2.68	-5.75	1.00	-3.07

The oxidation onset values of **L-PDPF**, **L-PDPF-O**, **Z-PDPF** and **Z-PDPF-O** versus an Ag electrode appear in 0.98, 0.80, 0.82 and 1.00 V, respectively. The band gaps of **L-PDPF**, **L-PDPF-O**, **Z-PDPF** and **Z-PDPF-O** are 3.00, 2.74, 2.81 and 2.68 eV, based on their onset oxidation potentials and the onset wavelength of their UV absorptions. These narrower band gaps after the oxidation clearly show that the cyclization can decrease the energy levels of the electronic migration in the conjugated backbone. Differences in band gaps and HOMO between the oligomers may originate from their different extents of conjugation, plus the band gaps show the same trend compared with the PL spectra red shift from **L-PDPF** and **Z-PDPF** to their oxides. The measured values match well with the shifts in optical measurements and are in agreement with the molecular magnified conjugated degree.

Afterwards the LCOs were applied as the semiconductor in FETs to measure their performance. The fascinating part is that the ion gel is used as the gate dielectric instead of some typical inorganic oxides like SiO_2, ZrO_2 and Al_2O_3.[56-59]The gate dielectric is another significant factor to influence the FET performance. Although some research groups have made several high-performance FETs with the inorganic dielectric, [60-62] the organic dielectric like ion gel possesses distinctive advantages. Besides the promising mechanical flexibility, the ion gel with an extraordinary high capacitance allows a low voltage operation to effectively diminish the heat generated by the devices.[63,64] Therefore the ion gel was chosen to combine the synthesized LCOs to fabricate the FETs in this work.

Fig. 6a is the photograph of the FET devices prepared by us, and the inserted 3D model simply displays the device structure of the thin film top-gate FET with ionic gel as the dielectric and aluminium as the gate layer. The obtained LCOs as the solution processing thin-film semiconductor were spin-coated on the Si/SiO_2 substrates. And the gold drain and source electrodes (typical channel length is 1000 μm with a width/length ratio of about 1) were vapor-deposited between the dielectric and the oligomer semiconductor layer. Fig. 6b and Fig. 6c show the typical output and transfer characteristic curves of the FET devices with **L-PDPF-O** as the semiconductor layer after thermal annealing at 150°C in a vacuum environment. Meanwhile, Fig. 6d and Fig. 6e show the same characteristic curves of the FET devices consist of **Z-PDPF-O**.

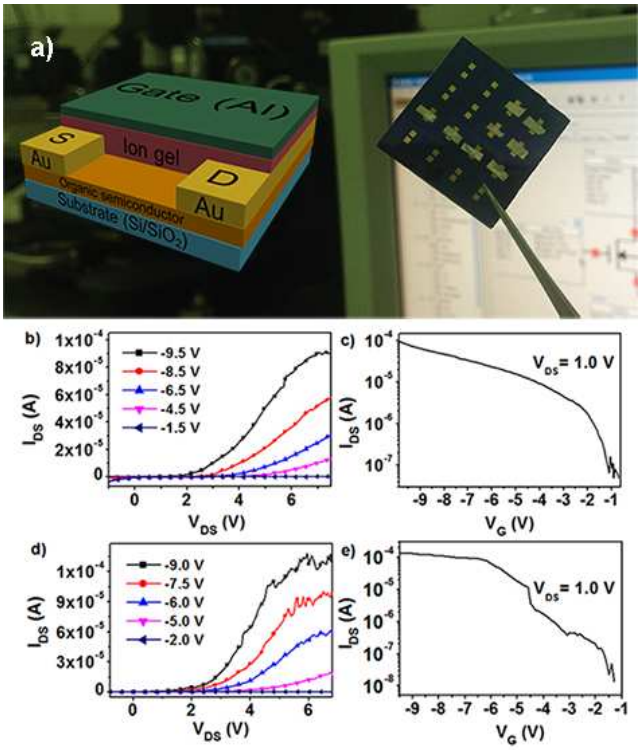

Fig. 6 (a) The photograph of the FETs, and the inserted 3D model shows the simple structure of this top-gate FET; (b) Output characteristics of the FETs consist of **L-PDPF-O**; (c) Transfer characteristic curve at V_{DS} = 1 V of the FETs consist of **L-PDPF-O**; (d) Output characteristics of the FETs consist of **Z-PDPF-O**; (e) Transfer characteristic curve at V_{DS} = 1 V of the FETs consist of **Z-PDPF-O**.

The output curves in Fig. 6b and Fig. 6d both confirm clear p-channel FET characteristics with the oligomer layer in devices. The key device parameters for these two devices, such as charge carrier mobility (μ) and on-to-off current ratio (I_{on}/I_{off}), are estimated from the drain-source current (I_{DS}) versus gate voltage (V_G) characteristics at V_{DS} = 1 V employing the metal-oxide semiconductor FET formula for the saturation regime:[65]

$$I_{DS} = \frac{\mu W C_i}{2L}(V_G - V_{TH})^2$$

Where W is the channel width, L is the channel length, C_i is the gate oxide capacitance per unit area, and V_{TH} is the threshold voltage. From a linear relationship between the $|I_{DS}|^{1/2}$ versus $|V_G|$ curve obtained at V_{DS} = 1 V (Fig. S32), V_{TH} of the devices with **L-PDPF-O** and **Z-PDPF-O** are evaluated to -1.0 V and -2.7 V respectively. C_i of the prepared ion gel is measured to be 20 μF/cm^2. The transfer characteristics have a low conductivity at the low V_G of around 0 V, which shows a promising air stability due to the low HOMO energy levels (-5.55 eV and -5.75 eV) of the obtained LCOs. According to V_{TH} and the transfer characteristics, the balanced value of μ for **L-PDPF-O** is 0.10 cm^{2}V^{-1}s^{-1} with an I_{on}/I_{off} of 2.1×10^3, and μ for **Z-PDPF-O** is 0.33 cm^{2}V^{-1}s^{-1} with an I_{on}/I_{off} of 8.2×10^3. Their excellent μ and I_{on}/I_{off} of the devices involving the obtained LCOs at a low operating voltage is a large advantage in the practical application of the organic FETs.

Conclusions

In summary, two well defined alternating co-oligomers **L-PDPF** and **Z-PDPF** consist of 9,9-dioctylfluorene and 1,2-diphenylethene have been successfully designed and synthesized via palladium-catalyzed Suzuki cross-coupling reaction in good yields. And so these two oligomers are exceptionally converted into the ladder-type conjugated oligomers **L-PDPF-O** and **Z-PDPF-O** by the anhydrous $FeCl_3$ oxidative cyclodehydrogenation, which presents a relatively straightforward solution processing method. This intramolecular cyclization is clearly corroborated by ^{1}H NMR and FTIR spectra of the oligomers and their model molecules. In addition, the preliminary photoluminescence spectra showing pronounced red shift and the changes of band gaps measured by electrochemical analysis, both testify that the expanded planarization of **L-PDPF-O** and **Z-PDPF-O** increases their electronic transmission capacity. Subsequently, the FET devices fabricated with the ladder-type conjugated oligomers as the semiconductor layer not only exhibit excellent air stability, but also possess good performance. Their mobilities are up to 0.10 cm^{2}V^{-1}s^{-1} and 0.33 cm^{2}V^{-1}s^{-1} respectively, showing the potential to conform to the actual requirements in the practical FETs application.

Additionally, we present the similarities and differences between the two precursor oligomers caused by the *cis-trans* isomerism linkage of 1,2-diphenylethene, which result in a linear and a zigzag shape chain: **L-PDPF** emits green light while **Z-PDPF** emits yellow light in the solid state; both of them possess excellent thermal properties and high fluorescent efficiency in solid films; **Z-PDPF** receives a glass transition at around 130 °C and 240 °C however **L-PDPF** doesn't show a clear glass transition, which may be owing to the easier rotation of the building blocks because of the more flexible zigzag chains; moreover, **Z-PDPF** displays obvious AIE phenomenon because the excited energy is mainly consumed by a nonradiative route like rotation of chains in solution while this nonradiative way is restrained in the solid state. The next studies in the future will take full advantage of the solution processing of the conjugated oligomer films to make high performance electrical

devices with some other fabricating techniques like ink-jet printing.[66,67]

Acknowledgements

This work was financially supported by the National Natural Science Foundation of China (21274027 and 20974022) and the Innovation Program of Shanghai Municipal Education Commission (15ZZ002).
H.J. Zhang thanks the FDUROP (Fudan's Undergraduate Research Opportunities Program) for support.

Notes and references

1 A. K. Geim and K. S. Novoselov, *Nat. Mater.*, 2007, ***6***, 183-191.
2 J. Wu, W. Pisula and K. Müllen, *Chem. Rev.*, 2007, ***107***, 718-747.
3 R. K. Joshi, P. Carbone, F. C. Wang, V. G. Kravets, Y. Su, I. V. Grigorieva, H. A. Wu, A. K. Geim and R. R. Nair *Science*, 2014, ***343***, 752-754.
4 S. Z. Butler, S. M. Hollen, L. Cao, Y. Cui, J. A. Gupta, H. R. Gutiérrez, T. F. Heinz, S. S. Hong, J. Huang, A. F. Ismach, E. Johnston-Halperin, M. Kuno, V. V. Plashnitsa, R. D. Robinson, R. S. Ruoff, S. Salahuddin, J. Shan, L. Shi, M. G. Spencer, M. Terrones, W. Windl and J. E. Goldberger, *ACS NANO*, 2013, *7*, 2898-2926.
5 Q. Liu, M. Cheng and G. Jiang, *Chem. Eur. J.*, 2013, ***19***, 5561- 5565.
6 X. Zhou, L. Wan and Y. Guo, *Chem. Commun.*, 2013, ***49***, 1838-1840.
7 G. Yu, L. Hu, M. Vosgueritchian, H. Wang, X. Xie, J. R. McDonough, X. Cui, Y. Cui and Z. Bao, *Nano Lett.*, 2011, ***11***, 2905-2911.
8 M. Lotya, Y. Hernandez, P. J. King, R. J. Smith, V. Nicolosi, L. S. Karlsson, F. M. Blighe, S. De, Z. Wang, I. T. McGovern, G. S. Duesberg and J. N. Coleman, *J. Am. Chem. Soc.*, 2009, ***131***, 3611-3620.
9 D. V. Kosynkin, A. L. Higginbotham, A. Sinitskii, J. R. Lomeda, A. Dimiev, B. K. Price and J. M. Tour, *Nature* 2009, ***458***, 872-876.
10 L. Tapasztó, G. Dobrik, P. Lambin and L. P. Biró, *Nat. Nanotechnol.*, 2008, ***3***, 397-401.
11 G. Srinivas, Y. Zhu, R. Piner, N. Skipper, M. Ellerby and R. Ruoff, *Carbon*, 2010, ***48***, 630-635.
12 M. Xu, T. Liang, M. Shi and H. Chen, *Chem. Rev.*, 2013, ***113***, 3766-3798.
13 B. Aufray, A. Kara, S. Vizzini, H. Oughaddou, C. Léandri, B. Ealet and G. Le Lay, *Appl. Phys. Lett.*, 2010, ***96***, 183102.
14 L. Zhi and K. Müllen, *J. Mater. Chem.,* 2008, ***18***, 1472-1484.
15 J. Ma, T. Lin, X. Pan and W. Wang, *Chem. Mater.*, 2014, ***14***, 4221-4229.
16 A. Narita, X. Feng, Y. Hernandez, S. A. Jensen, M. Bonn, H. Yang, I. A. Verzhbitskiy, C. Casiraghi, M. R. Hansen, A. H. R. Koch, G. Fytas, O. Ivasenko, B. Li, K. S. Mali, T. Balandina, S. Mahesh, S. De Feyter and K. Müllen, *Nat. Chem.*, 2013, ***6***, 126-132.
17 W. Zhang, X. Cao, H. Zi and J. Pei, *Org. Lett.*, 2005, *7*, 959-962.
18 L. Dou, J. You, J. Yang, C. Chen, Y. He, S. Murase, T. Moriarty, K. Emery, G. Li and Y. Yang, *Nat. Photonics*, 2012, ***6***, 180-185.
19 Y. Kim, S. Cook, S. M. Tuladhar, S. A. Choulis, J. Nelson, J. R. Durrant, D. D. C. Bradley, M. Giles, I. McCulloch, C. Ha and M. Ree, *Nat. Mater.*, 2006, ***5***, 197-203.
20 J. A. Letizia, M. R. Salata, C. M. Tribout, A. Facchetti, M. A. Ratner and T. J. Marks, *J. Am. Chem. Soc.*, 2008, ***130***, 9679-9694.
21 W. Wang, R. Wang, C. Zhang, S. Lu and T. Liu, *Polymer* 2009, ***50***, 1236-1245.
22 Z. Chen, M. J. Lee, R. S. Ashraf, Y. Gu, S. Albert-Seifried, M. M. Nielsen, B. Schroeder, T. D. Anthopoulos, M. Heeney, I. McCulloch and H. Sirringhaus, *Adv. Mater.*, 2012, ***24***, 647-652.
23 Y. Cao, Z. Guo, Z. Chen, J. Yuan, J. Dou, Y. Zheng, J. Wang and J. Pei, *Polym. Chem.*, 2014, ***5***, 5369-5374.
24 S. Thomas, I. Pinnau, N. Du and M. D. Guiver, *J. Membrane Sci.*, 2009, ***333***, 125-131.
25 W. Graupner, G. Leising, G. Lanzani, M. Nisoli, S. De Silvestri and U. Scherf, *Phys. Rev. Lett.*, 1996, ***76***, 847-850.
26 G. Zhou, M. Baumgarten and K. Müllen, *J. Am. Chem. Soc.*, 2008, ***130***, 12477-12484.
27 A. Babel and S. A. Jenekhe, *J. Am. Chem. Soc.*, 2003, ***125***, 13656-13657.
28 W. Zhang, Y. Liu and G. Yu, *Adv. Mater.*, 2014, ***26***, 6898-6904.
29 Y. Chen, C. Chang, Y. Cheng and C. Hsu, *Chem. Mater.*, 2012, ***24***, 3964-3971.
30 K. Takagi, Y. Ito, K. Kusafuka and M. Sakaida, *Org. Biomol. Chem.*, 2013, ***11***, 2245-2248.
31 H. H. Fan, L. Guo, K. F. Li, M. S. Wong and K. W. Cheah, *J. Am. Chem. Soc.*, 2012, ***134***, 7297-7300.
32 Y. Cheng, Y. Ho, C. Chen, W. Kao, C. Wu, S. Hsu and C. Hsu, *Macromolecules*, 2012, ***45***, 2690-2698.
33 J. Wencel-Delord and F. Glorius, *Nat. Chem.*, 2013, ***5***, 369-375.
34 M. Treier, C. A. Pignedoli, T. Laino, R. Rieger, K. Müllen, D. Passerone and R. Fasel, *Nat. Chem.*, 2010, ***3***, 61-67.
35 B. VanVeller, D. J. Schipper and T. M. Swager, *J. Am. Chem. Soc.*, 2012, ***134***, 7282-7285.
36 L. Dössel, L. Gherghel, X. Feng and K. Müllen, *Angew. Chem. Int. Edit.*, 2011, ***50***, 2540-2543.
37 A. Narita, I. A. Verzhbitskiy, W. Frederickx, K. S. Mali, S. A. Jensen, M. R. Hansen, M. Bonn, S. De Feyter, C. Casiraghi, X. Feng and K. Müllen, *ACS Nano*, 2014, ***8***, 11622-11630.
38 H. Arslan, F. J. Uribe-Romo, B. J. Smith and W. R. Dichtel, *Chem. Sci.*, 2013, ***4***, 3973-3978.
39 C. Reese, M. Roberts, M. Ling and Z. Bao, *Mater. Today*, 2004, 20-27.
40 C. Wang, H. Dong, W. Hu, Y. Liu and D. Zhu, *Chem. Rev.*, 2012, ***112***, 2208-2267.
41 M. Leclerc, *J. Polym. Sci. Pol. Chem.*, 2001, ***39***, 2867-2873.
42 U. Scherf and E. J. W. List, *Adv. Mater.*, 2002, *7*, 477-487.
43 D. Vak, J. Jo, J. Ghim, C. Chun, B. Lim, A. J. Heeger and D. Kim, *Macromolecules*, 2006, ***39***, 6433-6439.

44 Q. Hou, Q. Zhou, Y. Zhang, W. Yang, R. Yang and Y. Cao, *Macromolecules*, 2004, ***37***, 6299-6305.
45 G. Klärner, J. Lee, M. H. Davey and R. D. Miller, *Adv. Mater.*, 1999, ***11***, 115-119.
46 K. Ma, S. Li and R. G. Weiss, *Org. Lett.*, 2008, ***10***, 4155-4158.
47 T. Ishiyama, N. Matsuda, M. Murata, F. Ozawa, A. Suzuki and N. Miyaura, *Organometallics*, 1996, ***15***, 713-720.
48 M. Ranger, D. Rondeau and M. Leclerc, *Macromolecules*, 1997, ***30***, 7686-7691
49 N. Miyaura and A. Suzuki, *Chem. Rev.*, 1995, ***95***, 2457-2483.
50 P. Rempala, J. Kroulík and B. T. King, *J. Am. Chem. Soc.*, 2004, ***126***, 15002-15003.
51 C. D. Simpson, G. Mattersteig, K. Martin, L. Gherghel, R. E. Bauer, H. J. Räder and K. Müllen, *J. Am. Chem. Soc.*, 2004, ***126***, 3139-3147.
52 Y. Hong, J. W. Y. Lam and B. Z. Tang, *Chem. Soc. Rev.,* 2011, ***40***, 5361-5388.
53 H. Tong, Y. Hong, Y. Dong, M. Häußler, J. W. Y. Lam, Z. Li, Z. Guo, Z. Guo and B. Z. Tang, *Chem. Commun.*, 2006, 3705-3707.
54 F. Cacialli, R. Daik, W. J. Feast, R. H. Friend and C. Lartigau, *Opt. Mater.*, 1999, ***12***, 315-319.
55 A. C. Grimsdale, K. Leok Chan, R. E. Martin, P. G. Jokisz and A. B. Holmes, *Chem. Rev.*, 2009, ***109***, 897-1091.
56 L. Liao, J. Bai, Y. Lin, Y. Qu, Y. Huang and X. Duan, *Adv. Mater.*, 2010, ***22***, 1941-1945.
57 Y. Lin, K. A. Jenkins, A. Valdes-Garcia, J. P. Small, D. B. Farmer and P. Avouris, *Nano Lett.*, 2009, ***9***, 422-426.
58 C. Zhang, Y. Zang, E. Gann, C. R. McNeill, X. Zhu, C. Di and D. Zhu, *J. Am. Chem. Soc.*, 2014, ***136***, 16176-16184.
59 H. Wang, P. Wei, Y. Li, J. Han, H. R. Lee, B. D. Naab, N. Liu, C. Wang, E. Adijanto, B. C.-K. Tee, S. Morishita, Q. Li, Y. Gao, Y. Cui and Z. Bao, *P. Natl. Acad. Sci.*, 2014, ***111***, 4776-4781.
60 Y. Yuan, G. Giri, A. L. Ayzner, A. P. Zoombelt, S. C. B. Mannsfeld, J. Chen, D. Nordlund, M. F. Toney, J. Huang and Z. Bao, *Nat. Commun.*, 2014, ***5***, 1-9.
61 H. Okamoto, S. Hamao, H. Goto, Y. Sakai, M. Izumi, S. Gohda, Y. Kubozono and R. Eguchi, *Sci. Rep.*, 2014, ***4***, 1-6.
62 Y. S. Yang, T. Yasuda, H. Kakizoe, H. Mieno, H. Kino, Y. Tateyama and C. Adachi, *Chem. Commun.*, 2013, ***49***, 6483-6485.
63 J. H. Cho, J. Lee, Y. Xia, B. Kim, Y. He, M. J. Renn, T. P. Lodge and C. D. Frisbie, *Nat. Mater.*, 2008, ***7***, 900-906.
64 B. J. Kim, H. Jang, S. Lee, B. H. Hong, J. Ahn and J. H. Cho, *Nano Lett.*, 2010, ***10***, 3464-3466.
65 J. Shin, D. Kim, H. Park and G. Lim, *Electroanalysis*, 2004, ***16***, 1912-1918.
66 Y. Kim, B. Yoo, J. E. Anthony and S. K. Park, *Adv. Mater.*, 2012, ***24***, 497-502.
67 H. Wang, C. Cheng, L. Zhang, H. Liu, Y. Zhao, Y. Guo, W. Hu, G. Yu and Y. Liu, *Adv. Mater.*, 2014, ***26***, 4683-4689.

Table of Contents Graphic

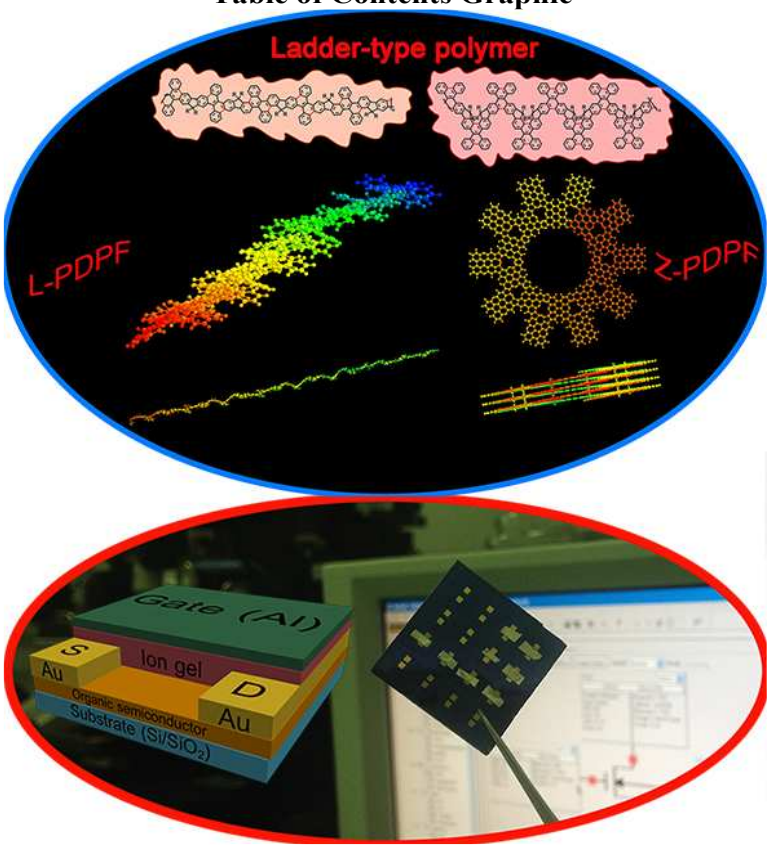

Two promising ladder-type conjugated oligomers are successfully designed and synthesized by the Scholl oxidative cyclodehydrogenation reaction. And the top-gate FET devices fabricated with the obtained oligomers as the semiconductor and the ion gel as the dielectric show excellent performance.